International Journal of Nanomedicine

Dovepress
Taylor & Francis Group

Open Access Full Text Article

ORIGINAL RESEARCH

Ginger-Derived Exosome-Like Nanoparticles: The Effect of Extraction Methods on Metabolites and in vitro Anti-Lung Cancer Activity

Tingwen Ming[1,*], Yang Yang[2,*], Jun Zhu[1], Juncheng Lin[1], Wang Yang[1], Guanbin Yu[1], Pengju Wang[1], Enxin Zhang[2], Qinhua Chen[2], Jingjian Liu[1,3]

[1]Sinopharm Dongfeng General Hospital, Hubei University of Medicine, Shiyan, 442008, People's Republic of China; [2]Shenzhen Bao'an Authentic TCM Therapy Hospital, Shenzhen, 518101, People's Republic of China; [3]Hubei Key Laboratory of Wudang Local Chinese Medicine Research, Hubei University of Medicine, Shiyan, 442000, People's Republic of China

*These authors contributed equally to this work

Correspondence: Qinhua Chen; Jingjian Liu, Email cqh77@163.com; liujj95@163.com

Introduction: In recent years, plant-derived exosome-like nanoparticles (PELNs) have attracted extensive attention. Among them, Ginger-derived exosome-like nanoparticles (GELNs) represent the most extensively studied category, demonstrating a wide spectrum of pharmacological activities. However, their specific efficacy against lung cancer remains largely unexplored and warrants further investigation. The appropriate isolation of GELNs is fundamental to all related research, yet a systematic comparison of different extraction methods is currently lacking. This study aimed to evaluate the differences among GELNs extracted by various methods and to investigate their anti-lung cancer pharmacological activities.

Methods: The study employed four common isolation methods—ultracentrifugation (UC), sucrose gradient UC (sgUC), membrane filtration, and polyethylene glycol-based precipitation (PEG-based precipitation) - to isolate GELNs. The GELNs were characterized by transmission electron microscopy (TEM), nanoparticle tracking analysis (NTA), and zeta potential measurements. Stability was evaluated under various conditions, including saline, serum, and different storage temperatures. The compositional profiles of GELNs extracted by four methods were explored using non-targeted metabolomics. A549 cells and PC-9 cells were used to assess the cellular uptake and anti-lung cancer efficacy of the four GELNs types. Network pharmacology, molecular docking, and molecular dynamics simulations were integrated to elucidate the potential mechanisms underlying their anti-lung cancer effects.

Results: The four methods successfully isolated GELNs with distinct profiles: UC achieved the highest protein yield (1.630 ± 0.022 g/kg), membrane filtration yielded the highest particle concentration (46.9 ± 6.71×10^8 particles/mL) but the lowest protein yield (0.059 ± 0.002 g/kg). Stability studies indicated that the highest stability of GELNs was observed for those isolated by UC and sgUC in both 0.9% and 10% NaCl. Furthermore, GELNs prepared by UC and membrane filtration showed excellent stability in serum. It was also demonstrated that −80°C provided the optimal storage condition for GELNs. Non-targeted metabolomics revealed the presence of 649 shared metabolites among the GELNs extracted by the four methods, along with method-specific unique metabolites. GELNs extracted by all four methods were internalized by both A549 and PC-9 cells. Among them, UC-isolated GELNs demonstrated the most potent anti-proliferative activity against the lung cancer cells. Through network pharmacology, 21 key targets of UC-isolated GELNs against lung cancer were identified. Molecular docking and molecular dynamics simulations further verified that 10-Gingerol, Hexahydrocurcumin, and [6]-Dehydrogingerdione from GELNs could stably bind to key targets, including Glycogen Synthase Kinase-3β (GSK3B), Progesterone Receptor (PGR), and SRC Proto-Oncogene, Non-Receptor Tyrosine Kinase (SRC).

Conclusion: This study demonstrates that although all four methods can isolate GELNs, UC is recommended for fundamental research due to its high protein yield, excellent stability, and potent in vitro anti-lung cancer activity. Furthermore, the anti-lung cancer activity of GELNs may be attributed to the regulation of GSK3B, PGR, and SRC by 10-Gingerol, Hexahydrocurcumin, and [6]-Dehydrogingerdione.

Keywords: ginger-derived exosome-like nanoparticles, extraction method, stability, metabolomics, lung cancer, network pharmacology

Received: 21 May 2025
Accepted: 22 October 2025
Published: 6 November 2025

Graphical Abstract

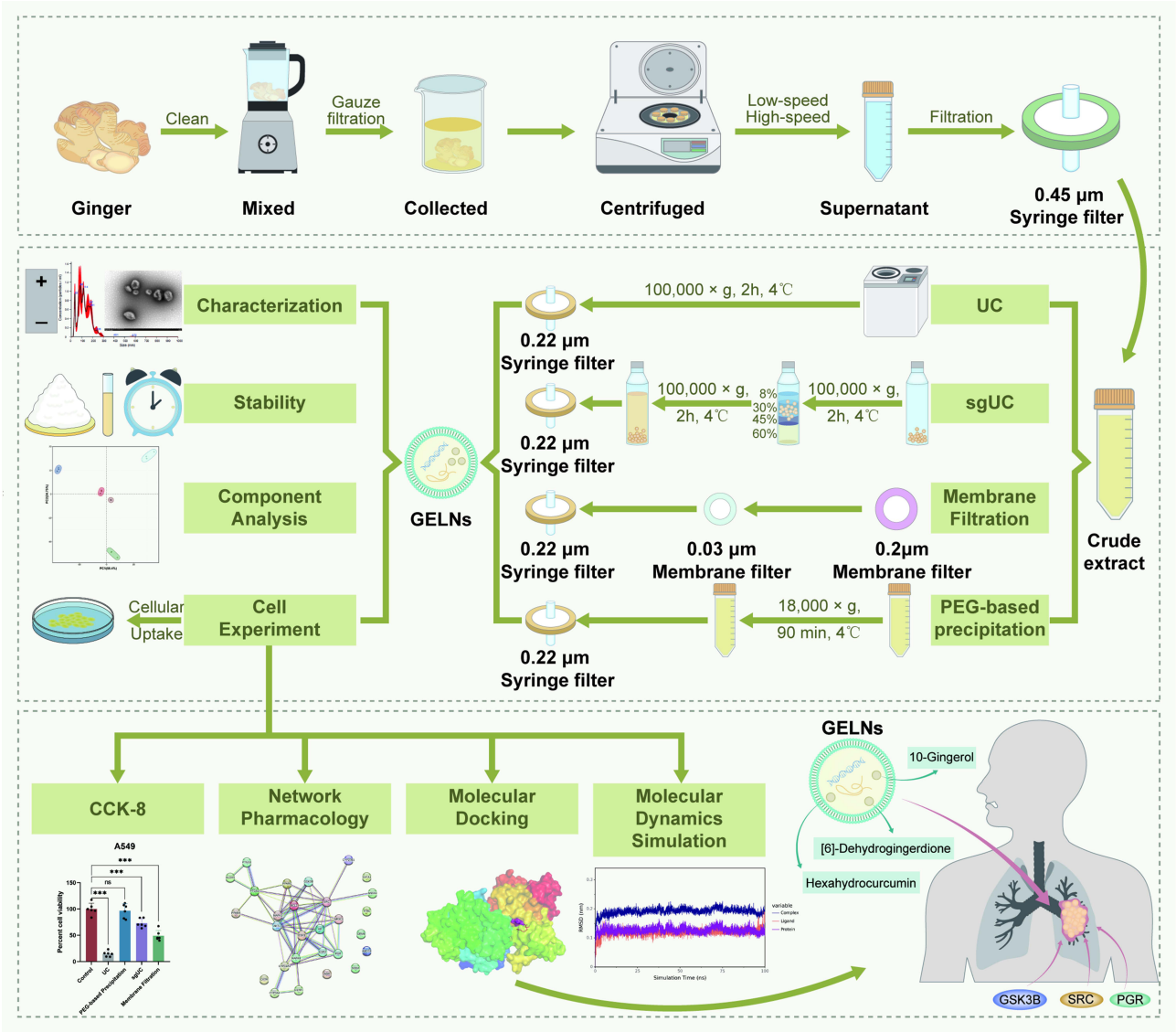

Introduction

Since their discovery in 1983 by Johnstone et al in cultured sheep reticulocytes, exosomes have been extensively studied.[1] These extracellular vesicles (EVs), typically 30 to 150 nm in diameter, are generated through an endocytosis-fusion-exocytosis mechanism.[2] They are ubiquitously present in diverse bodily fluids such as blood, urine, and milk and are laden with bioactive molecules, including proteins, lipids, DNA, and various non-coding RNAs.[3] Exosomes have been shown to play critical roles in a wide range of physiological and pathological processes.[4] The distinctive properties of exosomes, particularly their proficiency in crossing biological barriers, targeted trafficking, and innate role in disease regulation, have positioned them as a promising modality for nanotherapeutic development.[5] They can be applied directly or following engineering modification as therapeutic entities in their own right,[6] and they also serve as excellent drug delivery vehicles for nucleic acids, small molecules, and CRISPR/Cas systems.[7,8] Although exosomes demonstrate significant potential for disease treatment and cosmetic care, the clinical translation of mammalian-derived exosomes

(MEs) faces several formidable challenges. For instance, the isolation of exosomes from cell culture media suffers from low yield, high cost, and complex procedures, making it difficult to meet the demands of large-scale commercial production. Furthermore, their safety and immunogenicity pose significant concerns, as exosomes may carry pathogenic antigens from their parent cells, and their complex cargo constitutes an unpredictable biosafety hazard.[9]

In recent years, plant-derived exosome-like nanoparticles (PELNs) have emerged as a promising research focus. PELNs offer distinct advantages such as abundant sources, high yield, low cost, and diverse pharmacological activities.[10] They are enriched with natural bioactive lipids, proteins, RNAs, and other active molecules, which underpin their unique therapeutic potential.[11] Beyond those derived from traditional Chinese herbs, PELNs from common fruits and vegetables like ginger, tomato, and yam have also been extensively investigated.[12,13] Among the diverse PELNs being investigated, ginger-derived exosome-like nanoparticles (GELNs) stand out as the most extensively characterized, demonstrating a broad spectrum of pharmacological activities.[14] For instance, GELNs have been shown to alleviate osteoarthritis progression, prevent high-fat diet-induced insulin resistance, and exert anti-tumor effects by inducing apoptosis, cell cycle arrest, and inhibiting metastasis in triple-negative breast cancer MDA-MB-231 cells.[15–17] As research continues to expand, new therapeutic applications of GELNs are continually emerging. Lung cancer is the leading cause of cancer death among all cancers worldwide.[18] Currently, certain PELNs have been found to possess anti-lung cancer activity. For instance, nanoparticles derived from *Citrus limon* can suppress the proliferation of lung cancer A549 cells, while ginseng-derived exosomes alleviate immune evasion in non-small cell lung cancer by modulating PD-L1.[19,20] However, whether the GELNs have anti-lung cancer pharmacological activity remains unclear.

The efficient isolation and purification of GELNs represent a fundamental prerequisite for related research and a critical determinant for their future industrial-scale production. Current studies indicate that extraction methods significantly influence the physical characteristics and compositional profile of GELNs.[21] For instance, Man et al reported that GELNs isolated by Ultracentrifugation (UC) had an average size of 70.09 ± 19.24 nm, whereas those extracted by Zhang et al using a sucrose gradient ultracentrifugation (sgUC) protocol exhibited sizes of 292.5 nm, 231.6 nm, and 219.6 nm in different sucrose concentrations.[22,23] In the study by Zhang et al, the content of 6-gingerol and 6-shogaol within GELNs varied across different sucrose concentrations, which led to differential anti-inflammatory effects. However, no study has yet systematically investigated the impact of different extraction methods on GELNs. UC is the most fundamental and commonly used method for extracting GELNs. Additionally, techniques such as sgUC, membrane filtration, and polyethylene glycol precipitation (PEG-based precipitation) are also frequently employed for GELNs isolation.[21] Therefore, this study mainly selected these four methods for the extraction of GELNs.

In this study, GELNs were isolated using these four methods and characterized for their extraction efficiency, physical properties by transmission electron microscopy (TEM), nanoparticle tracking analysis (NTA), and dynamic light scattering (DLS), as well as for their stability in saline, serum, and upon storage. In addition, non-targeted metabolomics has been applied to analyze the composition of GELNs, aiming to evaluate the components of GELNs isolated by different methods. Finally, the cellular uptake and anti-proliferative activity against lung cancer cells of GELNs extracted by the different methods were evaluated. To further elucidate the anti-lung cancer mechanisms of GELNs, network pharmacology was first employed to preliminarily explore their potential mechanisms, given their complex composition.[24] This was followed by molecular docking and molecular dynamics (MD) simulations to further evaluate the binding of key active metabolites to lung cancer targets.[25] In summary, this study presents the first systematic comparison of GELNs extracted by four methods, focusing on their physical characteristics, yield, stability, metabolite composition, and in vitro anti-lung cancer pharmacological activity, to identify the optimal isolation method for different application scenarios. Additionally, it provides preliminary insights into their potential anti-lung cancer mechanisms. These findings are expected to offer a valuable reference for future research and development of GELNs.

Materials and Methods

Ginger Materials and Preprocessing

The fresh ginger roots used in this study were procured from Yunnan Province, China, and were authenticated as *Zingiber officinale* Roscoe by Prof. Hubiao Chen. A voucher specimen (Voucher number: HKBU-ZO-2024-003) has been

deposited at the Dr. and Mrs. Hung Hin Shiu Museum of Chinese Medicine, Hong Kong Baptist University.[26] After thoroughly cleaning the ginger root, it was used for the subsequent extraction of GLENs.

The pretreatment of ginger root was carried out as follows. Firstly, 500 mL of phosphate-buffered saline (PBS, pH 7.4, Beijing Solarbio Science & Technology Co., Ltd.) was added to sliced ginger root pieces (200g) and crushed for 5 min in the Joyoung JYL-C23 juicer (Joyoung Electric Appliance Co., Ltd., Jinan, China). Then, after filtering through double-layer sterile gauze (24–36 mesh, Winner Medical Co., Ltd.), the filtrate was centrifuged at 3200 × g for 90 min, 14,000 × g for 90 min, and 18,000 × g for 90 min at 4 °C (BY-R18, Beijing Baiyang Medical Equipment Co., Ltd., China). Finally, the obtained supernatant was filtered through a 0.45 μm syringe filter (Hunan BKMAM Holding Co., Ltd., China), and the GELNs were subsequently isolated using different methods.

Isolation of GELNs by Four Methods

UC, the most commonly employed method in exosome research, isolates exosomes based on their size and density through differential centrifugation at high speeds, thereby separating them from other components. 100 mL aforementioned ginger extract supernatant was centrifuged at 100,000 × g for 2 h at 4 °C using an Optima XE100 ultracentrifuge (Beckman Coulter, Brea, CA, USA). The resulting precipitate was dissolved in 2mL PBS, filtered through a 0.22 μm syringe filter (Hunan Bikeman Holding Co., Ltd., China), and stored at −80 °C for subsequent analysis.[27]

sgUC was often used as a supplement to UC to enhance the purity of isolated exosomes. Firstly, 8%, 30%, 45%, and 60% sucrose solutions were prepared and precooled at 4 °C. Subsequently, the precooled 60%, 45%, 30%, and 8% sucrose solutions were slowly layered sequentially into a centrifuge tube. 100 mL aforementioned ginger extract supernatant was then added, followed by centrifugation at 100,000 × g for 2 h at 4 °C. Immediately after centrifugation, the yellow band located between the 30% and 45% sucrose layers in the centrifuge tube was aspirated, and this fraction was ultracentrifuged again at 100,000 × g for 2 h at 4 °C. Finally, 2 mL PBS was added to resuspend the pellet, which was then filtered through a 0.22 μm syringe filter and stored at −80 °C for subsequent analysis.[28]

PEG-based precipitation was a simple method for exosome isolation that relies on the principle of chemical polymerization. A 20% (w/v) solution of PEG 6000 was prepared and pre-cooled to 4 °C. Subsequently, 100 mL aforementioned ginger extract supernatant was mixed with 100 mL pre-cooled 20% (w/v) PEG 6000 solution, followed by incubation at 4 °C for 24 h to facilitate GELNs precipitation. Following precipitation, the mixture was centrifuged at 18,000 × g for 90 min at 4 °C. Finally, the precipitate was resuspended in 2mL PBS, filtered through a 0.22 μm syringe filter, and stored at −80 °C for subsequent analysis.[29]

Membrane filtration was a method that separates exosomes based on their physical size. A volume of 100 mL of the aforementioned ginger extract supernatant was passed sequentially through 0.2 μm (Whatman Nuclepore Track-Etch Membrane, Cat. No.10417006) and 0.03 μm membrane filters (Whatman Nuclepore Track-Etch Membrane, Cat. No.110602) at a flow rate of 200 μL/min. The retentate was resuspended in PBS and filtered through a 0.22 μm syringe filter to a final volume of 2 mL, and stored at −80 ° C for subsequent analysis.

Characterization of GELNs

TEM was used to directly observe the morphology and size of GELNs. The prepared GELNs solution was applied to a clean sealing film. A carrier web (membrane-side down) was then placed on the droplet and left for 5 min to allow GELNs adsorption. After blotting the excess liquid, the carrier web was transferred onto uranyl acetate droplets for negative staining (2 min). The stained sample was blotted, air-dried, and examined by TEM (HT7800, Tokyo, Japan) at 12,000× magnification and 80.0 kV.

Nanosight NS300 (Malvern) was employed to determine the concentration and particle size distribution of GELNs. Specifically, 20 μL of GELNs were diluted to a final volume of 1 mL with PBS, then loaded into the sample chamber for analysis. The instrument parameters were set as follows: camera type, sCMOS; laser type, red laser; ambient temperature, 7.5 °C; viscosity parameter, water (1.4 cP); camera gain, 258–560; detection threshold, 2; number of single acquisition frames, 749. Each sample was measured in triplicate.

The zeta potential of GELNs was measured using a Nano ZS90 analyzer (Malvern) based on DLS. The GELNs sample was prepared by diluting 50 μL of the suspension to 1 mL with deionized water. Measurements were performed

in automatic mode (10–100 runs) at 25.0 °C after a 120 s thermal equilibration period. Each sample was analyzed in triplicate with no delay between measurements. The following parameters were applied: the material was modeled as polystyrene latex (refractive index = 1.590, absorbance = 0.010), and the dispersant was set as deionized water (viscosity = 0.8872 cP, refractive index = 1.330, dielectric constant = 78.5).

Stability Experiment

Protein concentration was quantified using a bicinchoninic acid (BCA) assay kit (Beyotime, Shanghai, China). GELNs extracted by various methods were adjusted to a protein concentration of 100 μg/mL using solvents such as PBS and saline. The storage stability of GELNs extracted by different methods was evaluated. The method for determining the zeta potential of GELNs by DLS was the same as described above. For measuring the particle size diameter of GELNs via DLS, the analysis was performed at 25°C with a detection angle of 90°, and the Z-average particle size was reported. The GELNs were stored at −80°C, −20°C, 4°C, and 25°C, and their particle size and zeta potential were measured by DLS on days 0, 7, 14, and 28. To investigate the stability in saline solution, GELNs separated by different methods were added to 0.9% (w/v) and 10% (w/w) saline solutions, respectively. These solutions were incubated at a constant temperature of 37 °C, and their particle size and zeta potential were measured by DLS at 0, 6, 12, and 24 h. For serum stability determination, GELNs extracted by different methods were added to fetal bovine serum (FBS, CellMax Biotechnology Co., Ltd., China) and incubated at 37 °C. The particle size and zeta potential were measured at 0, 6, 12, and 24 h, respectively.

Metabolomics Analysis

Firstly, 0.5 mL GELNs were slowly thawed at 4 °C and four times the volume of extraction solution (methanol/acetonitrile, 1:1, v/v) was added and homogenized for 60s. Subsequently, after 30 min of low-temperature ultrasonic extraction, the mixture was standing at −20 °C for 1 h to precipitate proteins. Then, the mixture was centrifuged at 12,000 rpm for 10 min at 4 °C, and the supernatant was dried under vacuum. Finally, 0.1 mL of a 30% acetonitrile solution was added and homogenized. The mixture was centrifuged at 12,000 rpm for 10 min at 4 °C, and the supernatant was collected for detection.

Chromatographic separation and analysis of the extracted supernatants were performed using an ultra-high-performance liquid chromatography (UPLC) system (Vanquish, UPLC, Thermo, USA). The supernatants were injected onto a Waters HSS T3 analytical column (100 mm × 2.1 mm, 1.8 μm), with the column temperature maintained at 40 °C and a constant flow rate of 0.3 mL/min. The analytical conditions were set as follows: The mobile phase consisted of water containing 0.1% acetic acid (phase A) and acetonitrile containing 0.1% acetic acid (phase B). The gradient elution program was as follows: 0 min, 100:0 (A: B, v/v); 1 min, 100:0 (A: B, v/v); 4 min, 40:60 (A: B, v/v); 6.5 min, 5:95 (A: B, v/v); 6.6 min, 100:0 (A: B, v/v); 8.0 min, 100:0 (A: B, v/v).

High-throughput mass spectrometric data acquisition was conducted using a Q Exactive HFX Hybrid Quadrupole Orbitrap mass spectrometer, which was equipped with a dual-channel electrospray ionization (ESI) source operated in both positive and negative ion modes. The operational parameters of the ESI source were set as follows: sheath gas pressure, 40 arb; auxiliary gas pressure, 10 arb; spray voltage, +3000 V/−2800 V; capillary temperature, 350 °C; and ion transfer tube temperature, 320 °C. For the mass spectrometric scanning, the full-scan MS (primary mass spectrometry) was configured with a scan range of 70–1050 Da, along with a resolution of 70,000 for full-scan MS (primary MS) and 17,500 for MS/MS (secondary MS).[30]

Cell Culture

The lung cancer A549 and PC-9 cell lines were obtained from Procell Life Science & Technology Co., Ltd. (Wuhan, China). A549 cells were cultured in F-12K medium (Meisen Biotechnology Co., Ltd., MeisenCTCC, China) supplemented with 10% FBS and 1% penicillin-streptomycin (CellMax Biotechnology Co., Ltd., China) in a constant-temperature incubator at 37°C with 5% CO_2. PC-9 cells were cultured in RPMI 1640 Basal Medium (Gibco, Carlsbad, CA, USA) under the same supplementation and incubator conditions as A549 cells.

Uptake of GELNs

The effective cellular internalization of GELNs was a prerequisite for exerting anti-lung cancer effects. The cellular uptake of GELNs extracted by the four methods was evaluated using fluorescence localization. A549 cells and PC-9 cells were seeded in a 24-well plate at a density of 2×10^4 cells per well. GELNs isolated via the four extraction methods were labeled using the BeyoExo™ Labeling and Tracking Kit (PKH67, Beyotime, Cat. No. C3635S), following the manufacturer's instructions.[31] After the cells adhered to the plate surface, the labeled GELNs were added to each well to achieve a final concentration of 100 μg/mL. The plate was incubated at 37 °C in a cell incubator for 8 h, after which the cells were rinsed twice with PBS. Subsequently, 0.5 mL of 4% paraformaldehyde (Servicebio, Cat. No. G1101-500ML, Wuhan, China) was added to each well to fix the cells for 30 min. After fixation, each well was treated with 0.5 mL of PBS containing 0.1% Triton X-100 (Beyotime, Cat. No. P0096-100ML), followed by two washes with PBS. Next, Actin-Tracker Red-Rhodamine (Beyotime, Cat. No. C2207S), prepared at a 1:200 dilution, was used to stain the cellular cytoskeleton.[32] Following 20 min of staining, the cells were washed twice more with 0.5 mL of PBS supplemented with 0.1% Triton X-100. 0.5 mL of Hoechst 33258 working solution (1 mg/mL, Wuhan AntGene Biotechnology Co., Ltd.) was added to each well, and the plate was incubated in the dark for 30 min to stain cell nuclei. Finally, the cells were rinsed twice with PBS, and cell images were captured at 200 × magnification (20 × objective, 10 × eyepiece) using an inverted fluorescence microscope (OLYMPUS CKX71). All captured images were further processed using ImageJ software.

Cell Viability Assay

The inhibitory effect of GELNs extracted by four methods on lung cancer cells was assessed using the Cell Counting Kit-8 (CCK-8) assay. A549 and PC-9 cells were seeded separately in 96-well plates at a density of 1×10^4 cells/well and incubated overnight. The control group was cultured in standard medium, while the experimental groups were treated with 100 μg/mL GELNs isolated via different extraction methods. After 24 h of incubation at 37°C, the culture medium in each well was carefully aspirated, and all wells were rinsed twice with PBS. Subsequently, 100 μL of fresh medium containing 10% CCK-8 reagent (TargetMol, Boston, MA, USA) was added to each well, followed by incubation at 37°C for 2 h. The absorbance at 450 nm was detected using a full-wavelength microplate reader (Biotek MQX200), and cell viability was calculated and visualized with GraphPad Prism 8.0.1.

Network Pharmacology Analysis

The PubChem ID numbers of the top 20 most abundant active metabolites in GELNs isolated by UC were input into the BATMAN-TCM database (version 2.0; http://bionet.ncpsb.org.cn/batman-tcm/) to predict potential target genes.[33] The screening criteria were set as a confidence score threshold of > 0.80 (likelihood ratio, LR = 48) and $P < 0.05$. Lung cancer-related genes were initially retrieved from the GeneCards database (http://www.genecards.org/) and Online Mendelian Inheritance in Man (OMIM) database (https://www.omim.org/) by searching with the keyword "Lung cancer". Genes obtained from GeneCards (with a relevance score > 20) and OMIM were then integrated, with duplicate entries removed, to define core lung cancer-related genes. Subsequently, the core genes of GELNs were then intersected with the core lung cancer-associated genes using a Venn diagram tool on the Weishengxin online platform (http://113.44.3.163) to identify the key genes potentially mediating the effects of GELNs on lung cancer.

The key genes were submitted to the STRING database (http://string-db.org) to construct a protein-protein interaction (PPI) network. The analysis was restricted to *Homo* sapiens with a minimum interaction confidence score of 0.7. The resulting PPI data were imported into Cytoscape software (version 3.10.1) for topological analysis. The network was visualized and ranked based on the "degree". Gene Ontology (GO) and Kyoto Encyclopedia of Genes and Genomes (KEGG) pathway enrichment analyses for the key genes were performed using the DAVID database (https://david.ncifcrf.gov/). The parameters were set as follows: identifier, OFFICIAL_GENE_SYMBOL; species, *Homo* sapiens; list type, Gene List. Enrichment in GO terms-including biological process (BP), cellular component (CC), and molecular function (MF), and KEGG pathways was analyzed. And the results were sorted by *p*-value and visualized.

Further screening of key genes was conducted through survival analysis. Lung cancer was selected as the research subject for analysis in the mRNA microarray module of the KM plotter database (https://kmplot.com/analysis/).[34] Kaplan-Meier (KM) survival curves were constructed by inputting key genes, with a 60-month follow-up threshold established for both analytical processes and result visualization. Subsequently, genes exhibiting a close association with lung cancer were screened out to serve as candidates for subsequent in-depth investigation.

Molecular Docking

Molecular docking was performed to predict the binding affinity between the key genes significantly associated with lung cancer prognosis and the major active metabolites in GELNs. The 3D structures of the target proteins were downloaded in PDB format from the RCSB Protein Data Bank database (https://www.rcsb.org/). The 3D structures of the metabolites were downloaded in SDF format from the PubChem database (https://pubchem.ncbi.nlm.nih.gov/) and converted to PDB format using OpenBabel (version 2.4.1). Molecular docking was performed utilizing the CB-Dock2 online analysis platform.[35] The docking module was selected for molecular docking assays, with PDB-formatted files of small molecules and proteins inputted for simulation. From five independent simulation runs, the result with the most favorable binding energy was chosen as the outcome. The PDB file of the docking results was downloaded and visualized using PyMOL software.

Molecular Dynamics Simulation

MD simulations were performed using the GROMACS 2022.[36] The AMBER14SB force field was applied to the protein, the GAFF force field to the small-molecule ligands, and the TIP3P model was used for water molecules. The files of proteins and small-molecule ligands were merged, and a simulation system of the complex was constructed. Bonds involving hydrogen atoms were constrained using the LINCS algorithm, allowing for an integration time step of 2 fs. The electrostatic interactions were calculated using the Particle-mesh Ewald method, with a cutoff value of 1.2 nm. The nonbonded interaction cutoff was set to 10 Å with the neighbor list updated every 10 steps. The system temperature was maintained at 298 K using the V-rescale thermostat, and the pressure was controlled at 1 bar using the Berendsen barostat. At a constant temperature of 298 K, 100 ps of NVT equilibrium simulation and 100 ps of NPT equilibrium simulation were performed sequentially. This was followed by a 100 ns MD simulation of the complex system, during which the coordinates were saved every 10 ps. The resulting trajectory was analyzed upon simulation completion using Visual Molecular Dynamics (VMD) and PyMOL.

Statistical Analysis

In this study, data analysis was performed using GraphPad Prism software (version 8.0.1). Data from three independent experiments were expressed as the mean ± standard deviation. The normality of the data distribution was assessed using the Shapiro–Wilk test. For data conforming to a normal distribution, statistical comparisons between groups were made using an unpaired two-tailed *t*-test or one-way analysis of variance (ANOVA), with a probability value of $*p < 0.05$ considered statistically significant.

Results

Comparison of Isolation Efficiency and Physical Characteristics

For each independent batch preparation, GELNs were isolated from the root tissue of one individual ginger plant to guarantee uniformity in the starting material. Following isolation, the GELNs were characterized by TEM, NTA, and DLS to evaluate their isolation efficiency and physical characteristics. The morphology of GELNs was first examined by TEM. As shown in Figure 1A, D, G and J, GELNs isolated using all four methods exhibited relatively intact structures with morphological characteristics analogous to animal exosomes. Specifically, the GELNs presented cup-shaped, discoid, or oval morphologies, bounded by a distinct lipid bilayer visible as a bright outer layer and a darker inner core.

NTA was employed to further determine the size distribution of GELNs. As shown in Figure 1B, E, H, K and Table 1, the average particle size of GELNs isolated by the four methods was approximately 120 nm, with most particles

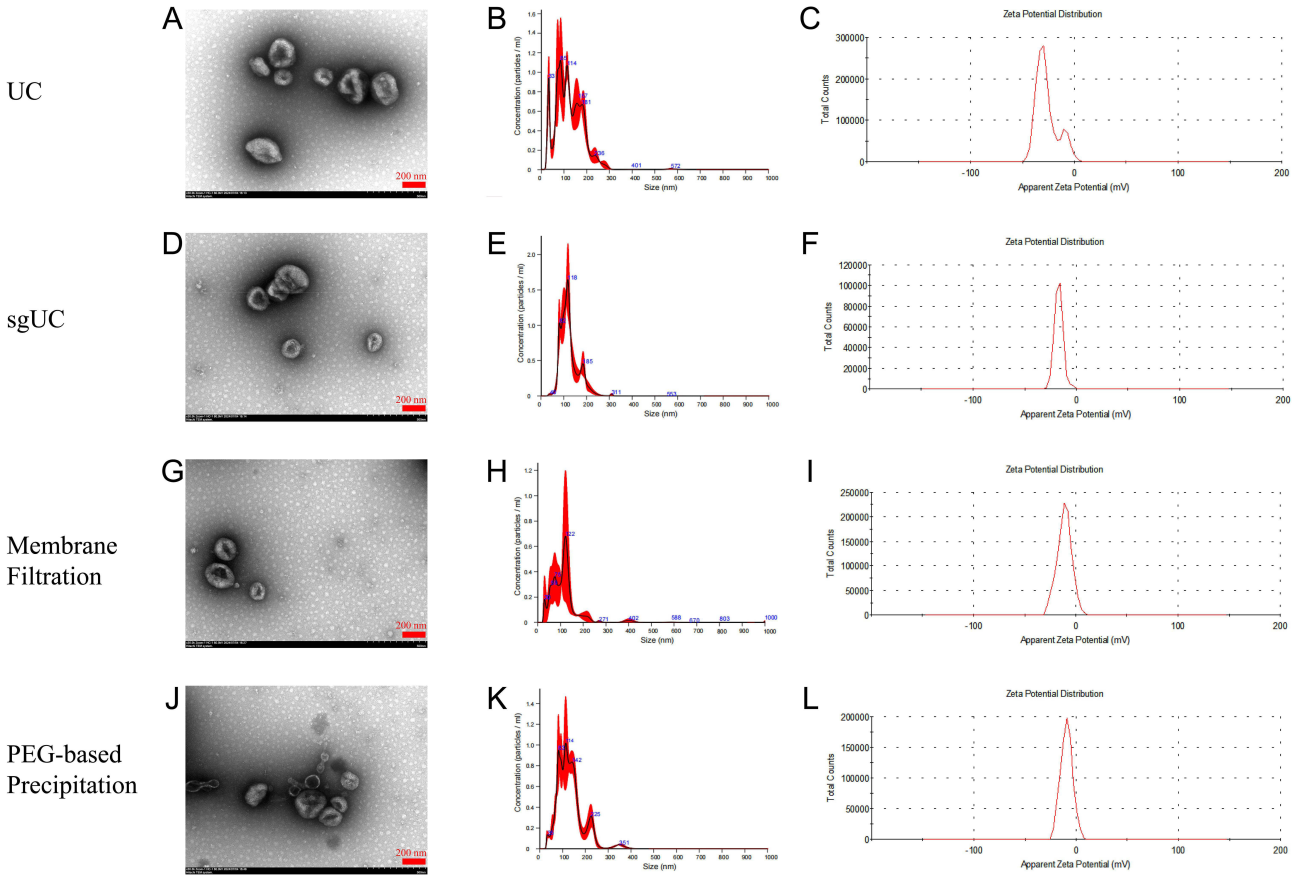

Figure 1 Characterization of GELNs isolated by four methods (UC, sgUC, membrane filtration, and PEG-based precipitation). (**A, D, G** and **J**) The TEM image of GELNs (scale bars = 200 nm). (**B, E, H** and **K**) The NTA of GELNs. (**C, F, I** and **L**) The Zeta potential measurement of GELNs.

distributed in the range of 30–150 nm. Despite a 50-fold dilution of GELN samples before detection, all four methods yielded GELNs with high concentrations. Among these techniques, membrane filtration-isolated GELNs exhibited the highest concentration.

The zeta potentials of the GELNs isolated by the four methods were measured and presented in Figure 1C, F, I and L. The values recorded were: UC, −26.37 ± 1.22 mV; sgUC, −17.0 ± 0.29 mV; membrane filtration, −11.03 ± 0.33 mV; and PEG-based precipitation, −9.3 ± 0.67 mV. All measured zeta potentials fell within the characteristic range reported for PELNs.[21]

Overall, all four methods were able to successfully isolate GELNs. The yields of GELNs extracted by the four methods were calculated, among which the UC method yielded the highest amount of GELNs (1.630 ±0.022 g/kg), followed by sgUC (1.255±0.008 g/kg) and PEG-based precipitation (1.261±0.022 g/kg), while the membrane filtration method yielded the lowest amount of GELNs (0.059±0.002 g/kg) (Figure 2A). It should be noted that the yield reported here refers to the protein concentration of the exosomes extracted from ginger roots.

Table 1 NTA Comparison of Four Methods for Extracting the GELNs

GELNs	UC	sgUC	Membrane Filtration	PEG-Based Precipitation
Average particle size (nm)	123.20 ± 2.20	123.80 ± 1.00	108.60 ± 21.00	133.10 ± 6.80
Total concentration ($1*10^8$)	13.40±0.59	10.20±0.28	46.90±6.71	10.60±1.45
Percentage of particle size 30–150 nm (%)	64.36 ± 0.99	78.22± 2.97	84.80 ± 7.12	69.64± 8.42
Percentage of particle size 150–200 nm (%)	23.43 ± 1.51	16.50 ± 2.29	6.28 ± 2.04	15.84 ± 0.99

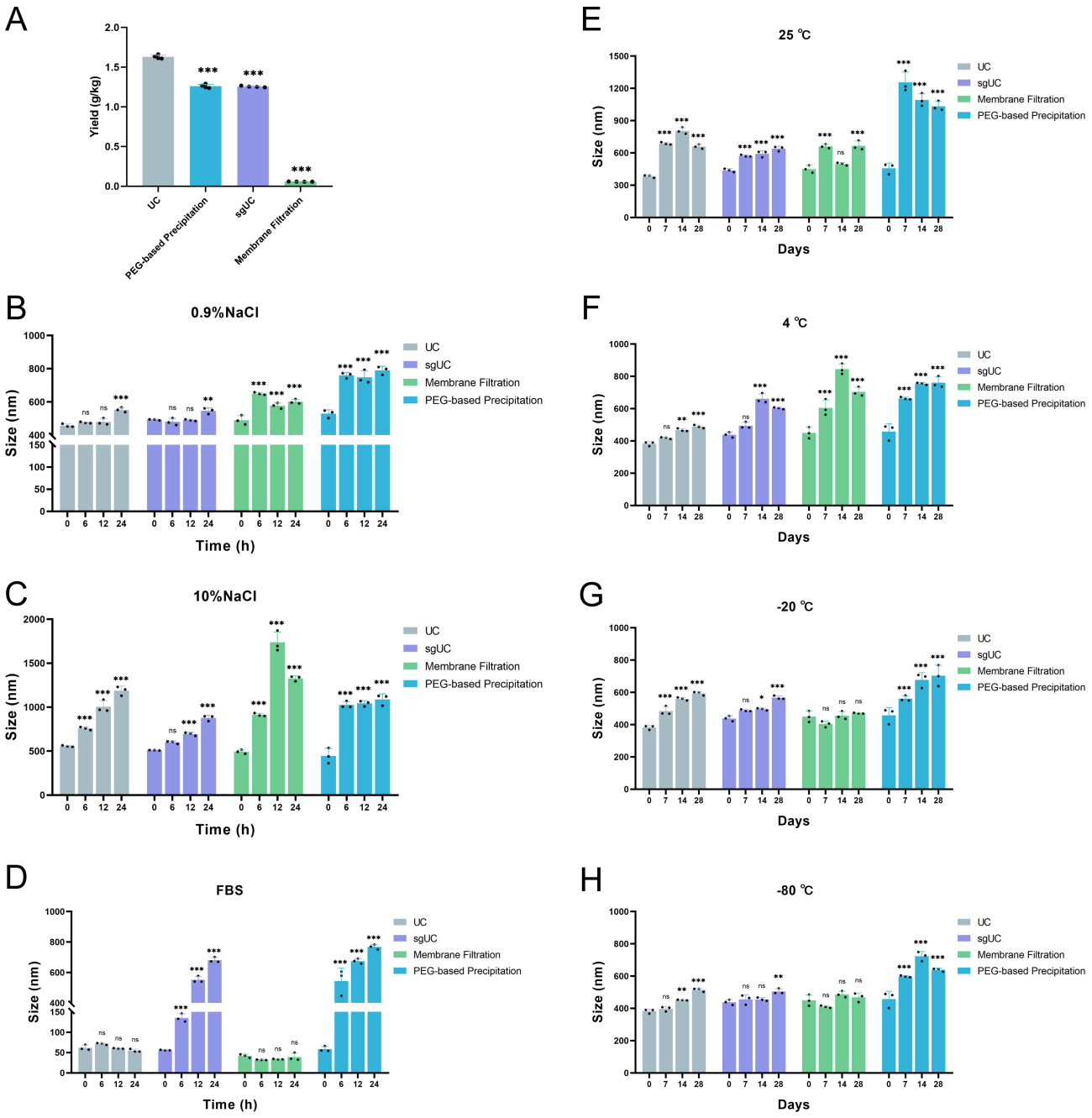

Figure 2 Compare the yield and stability of GELNs isolated by four methods. (**A**) Extraction yield of GELNs, expressed as grams of exosomal protein per kilogram of fresh ginger root (g/kg) (n = 4, ***$p < 0.001$, the yield of GELNs isolated by sgUC, membrane filtration and PEG-based precipitation compared with UC). (**B**–**D**) Particle size dynamics of GELNs isolated by the four methods under different solvent conditions ((**B**) 0.9% NaCl, (**C**) 10% NaCl, (**D**) FBS) over time. Data and statistical comparisons for each method are presented relative to its respective 0-time control within the same solvent group (n = 3, ns: non-significant, **$p < 0.01$, ***$p < 0.001$). (**E**–**H**) Particle size dynamics of GELNs isolated by the four methods under different temperature conditions ((**E**) 25°C, (**F**) 4°C, (**G**) −20°C, (**H**) −80°C) over time. Data and statistical comparisons for each method are presented relative to its respective 0-time control within the same solvent group (n = 3, ns: non-significant, *$p < 0.05$, **$p < 0.01$, ***$p < 0.001$).

Stability of GELNs Isolated by Different Methods

First, we investigated the stability of GELNs isolated by the four methods in 0.9% NaCl and 10% NaCl over 24 h. In 0.9% NaCl, the particle size of GELNs isolated by both UC and sgUC showed no significant change from 0 to 12 h but increased significantly at 24 h (Figure 2B). In contrast, GELNs obtained via membrane filtration and PEG-based precipitation exhibited a significant increase in size as early as 6 h. Regarding the surface charge, the zeta potential of

https://doi.org/10.2147/IJN.S541948

GELNs isolated by all four methods remained generally stable after incubation in 0.9% NaCl (Figure S1A). When the GELNs isolated by the four methods were placed in 10% NaCl, the particle size increased across all groups (Figure 2C). The zeta potential of GELNs isolated by UC and sgUC remained generally stable overall. In contrast, the zeta potential of those isolated by membrane filtration and PEG-based precipitation became more negative (Figure S1B).

Interestingly, when GELNs isolated by the four methods were introduced into FBS, their particle sizes, as determined by DLS, reverted to the typical exosome size range (30–150 nm). For GELNs isolated by UC and membrane filtration, the particle size showed no significant change within 24 h. In contrast, the particle size of GELNs obtained via sgUC and PEG-based precipitation gradually increased over time (Figure 2D). Zeta potential data indicated that GELNs isolated by UC and membrane filtration remained relatively stable in the FBS environment (Figure S1C). The stability of GELNs isolated by the four methods was evaluated under different storage temperatures. Results indicated that particle size increased and the absolute value of the zeta potential decreased across all preparations over time (Figures 2E–H and S1D–G). Overall, storage at −80°C resulted in the minimal changes in both parameters, identifying it as the optimal condition for preserving the stability of GELNs.

Comparison of GELNs Components Based on Metabolomics

Non-targeted metabolomics was used to analyze GELNs isolated by four methods. Figure S2 shows representative base peak chromatograms (BPC) obtained from quality control (QC) samples in positive and negative ionization modes, evaluating the performance of the UPLC-MS/MS platform and the quality of the acquired data. The chromatograms exhibit numerous well-resolved peaks with high signal intensity and a stable baseline, confirming excellent chromatographic separation, high sensitivity, and system stability. Principal component analysis (PCA) was employed to assess the overall metabolic differences among sample groups and the variability within them. As shown in Figure 3A, the distinct clustering of the samples, characterized by tight intra-group aggregation and clear inter-group separation, was observed. The high degree of aggregation of the QC samples confirms the stability of the analytical system and the reliability of the acquired data. Figure 3B further illustrates the similarity of each sample. Figure 3C displays the number of detected metabolites in the four sample groups and further analyzes the overlap and uniqueness of metabolites among them using a Venn diagram. Among them, 649 metabolites were shared across all four sample groups, while each group also possessed its own unique metabolites. Metabolite analysis revealed that a core set of metabolites was consistently identified in GELNs extracted by all four methods, including 10-Gingerol, 4-Gingerdiol, 6-Gingerdiol, and others. Figure 4D shows the main categories of the GELNs metabolites, including Prenol lipids, Organooxygen compounds, Fatty Acyls, Steroids and steroid derivatives, Carboxylic acids and Derivatives, Phenols, and Flavonoids.

To further illustrate the compositional differences of GELNs isolated by the four methods, Figure S3A–D presents the top 10 most abundant metabolites for each extraction method. The variation in key metabolites, notably (10)-Gingerol and 1-Dehydro-6-gingerdione, across GELNs obtained by four methods represents a potential driver for the method-dependent differences in pharmacological activity. GELNs extracted by the UC method served as the control, against which the metabolic profiles of GELNs isolated by the other methods were assessed. Metabolites were considered differential in the volcano plot using the criteria of Fold Change (FC) > 1.5 or FC < 0.67 combined with a P value < 0.05 (Figure 4A, C and E). Figure 4B, D and F illustrate the top 20 most significantly altered metabolites ranked by the magnitude of their FC. Collectively, these results demonstrate distinct differences in the metabolite composition and abundance of GELNs extracted by the four methods.

In vitro Cellular Uptake and Anti-Lung Cancer Activities of GELNs

Successful cellular uptake of GELNs is a fundamental prerequisite for their pharmacological activity. Figure 5A and B present representative images of the uptake of GELNs, isolated by the four methods, by A549 and PC-9 cells, respectively. The results indicated that GELNs extracted by all four methods were efficiently internalized by both A549 and PC-9 cells and were primarily localized in the cytoplasm. To further evaluate the impact of GELNs extracted by the four methods on lung cancer cell proliferation, a CCK-8 assay was performed. The results in Figure 6A and B demonstrate that GELNs isolated by methods other than PEG-based precipitation significantly inhibited the

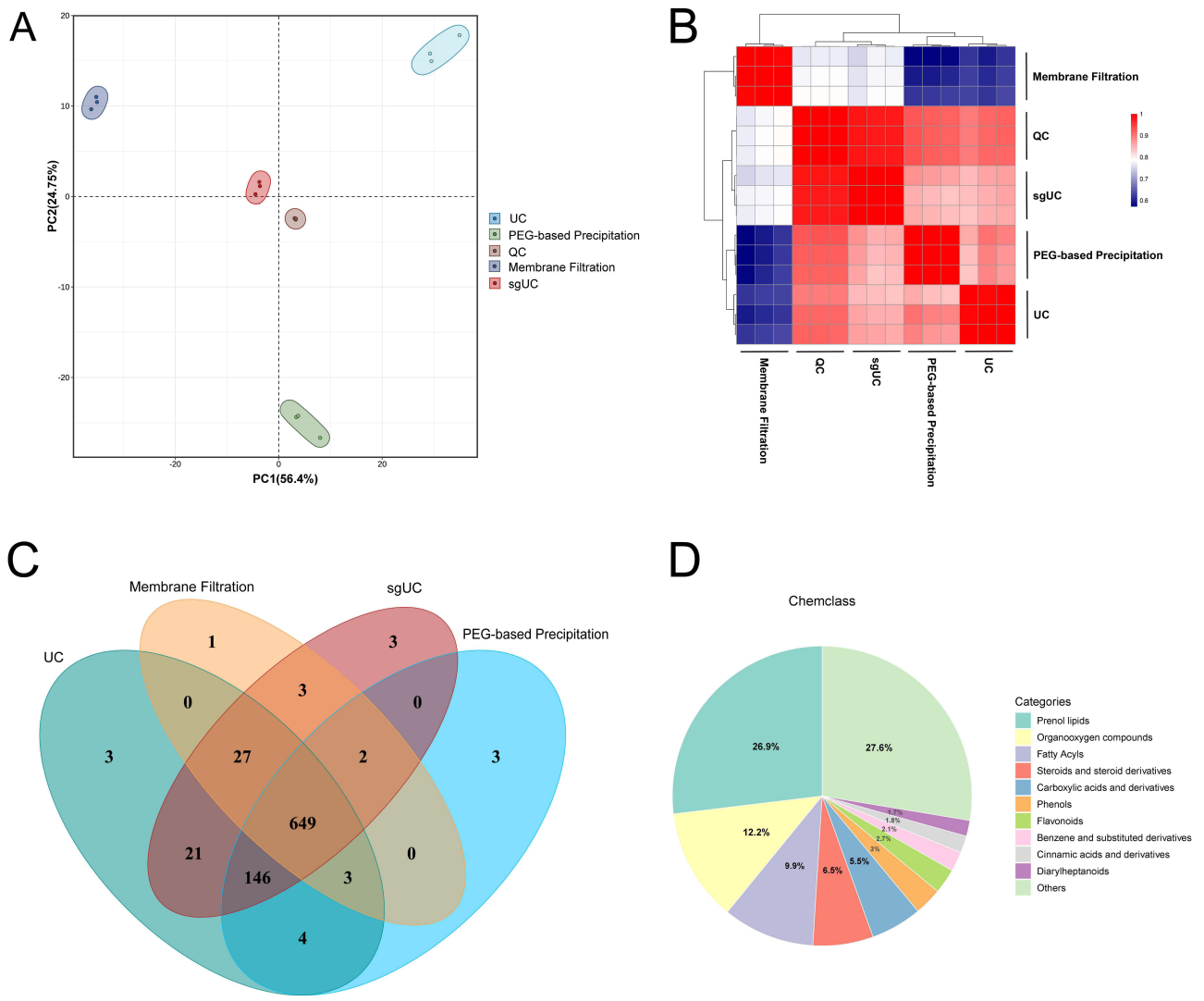

Figure 3 Comparison of metabolites in GELNs extracted by four methods. (**A**) The PCA score map. (**B**) The Heatmap of sample similarity. (**C**) The Venn diagram of differences in GELNs metabolites. (**D**) Pie chart of metabolite classification (n=3).

proliferation of A549 and PC-9 cells, with UC-isolated GELNs showing the most potent effects. Conversely, PEG-precipitated GELNs were inactive at this concentration, likely due to inherent limitations of the method, including residual polymers and potential false-positive signals.

Network Pharmacology Analysis of the Anti-Lung Cancer Mechanism of Ultracentrifugation-Isolated GELNs

Network pharmacology was employed to further investigate the mechanism of GELNs against lung cancer. Here, the metabolomic data of UC-isolated GELNs were utilized for the screening of relevant targets. The top 20 metabolites with the highest relative abundance in GELNs were analyzed using the BATMAN-TCM database, leading to the identification of 10 key metabolites and their corresponding 124 target genes. As shown in Table 2, the key metabolites of GELNs include representative ginger-derived substances such as 10-gingerol and [6]-Dehydrogingerdione. These anti-tumor active metabolites are hypothesized to serve as the material basis for GELNs to exert anti-lung cancer efficacy. Following the further confirmation of the main components in GELNs, network pharmacology was utilized to dissect the mechanism underlying their anti-lung cancer activity.

https://doi.org/10.2147/IJN.S541948

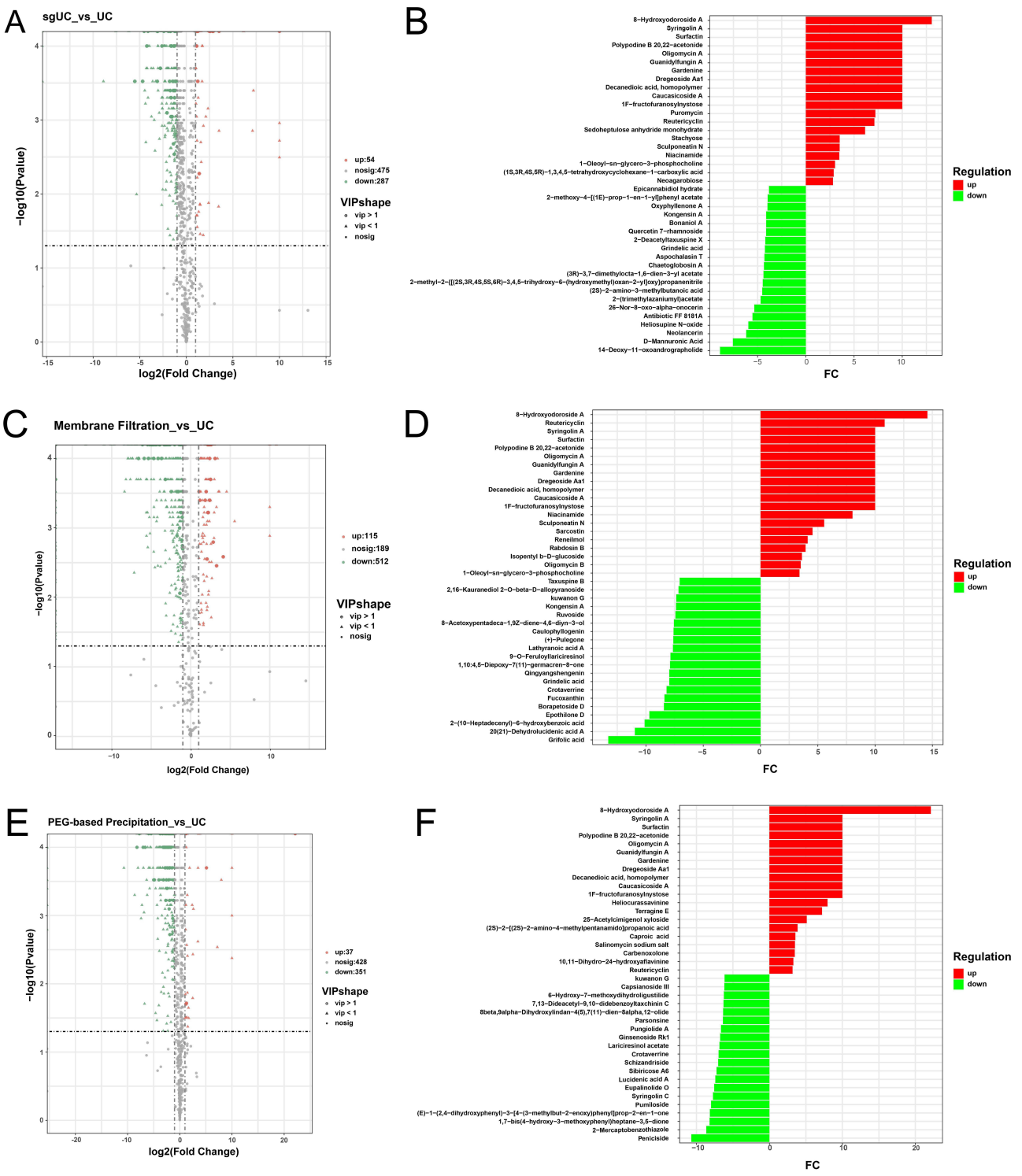

Figure 4 Comparative analysis of differential metabolites in GELNs extracted by four methods: sgUC, membrane filtration, PEG-based precipitation, and UC. (**A, C** and **E**) The volcano plots of differential metabolites. (**B, D** and **F**) The Bar chart of the top 20 metabolites with the most significant fold changes for the respective comparisons (n=3, Metabolites detected in GELNs isolated by sgUC, membrane filtration, and PEG-based precipitation were compared to those isolated by UC).

As illustrated in Figure 6C, a total of 1991 lung cancer-related targets were retrieved from the GeneCards and OMIM databases. Subsequently, these targets were intersected with the target genes derived from GELNs, yielding 28 common targets. A protein-protein interaction (PPI) network was then constructed for these common targets (Figure 6D). Topological analysis was then performed to identify 21 lung cancer key targets, which were ranked according to their

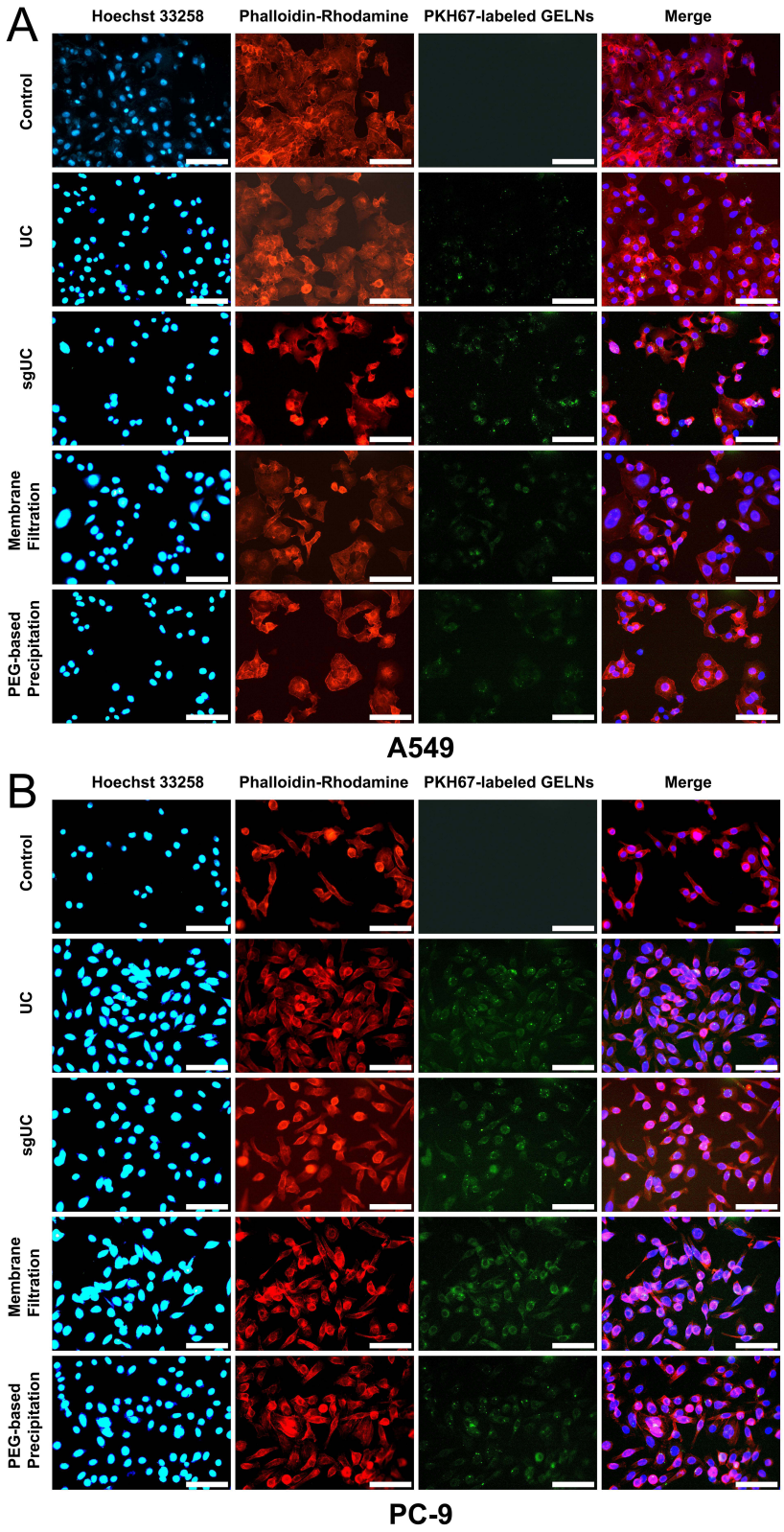

Figure 5 Confocal fluorescence imaging shows internalization of GELNs in A549 cells (**A**) and PC-9 cells (**B**), respectively (scale bars = 100 μm).

https://doi.org/10.2147/IJN.S541948

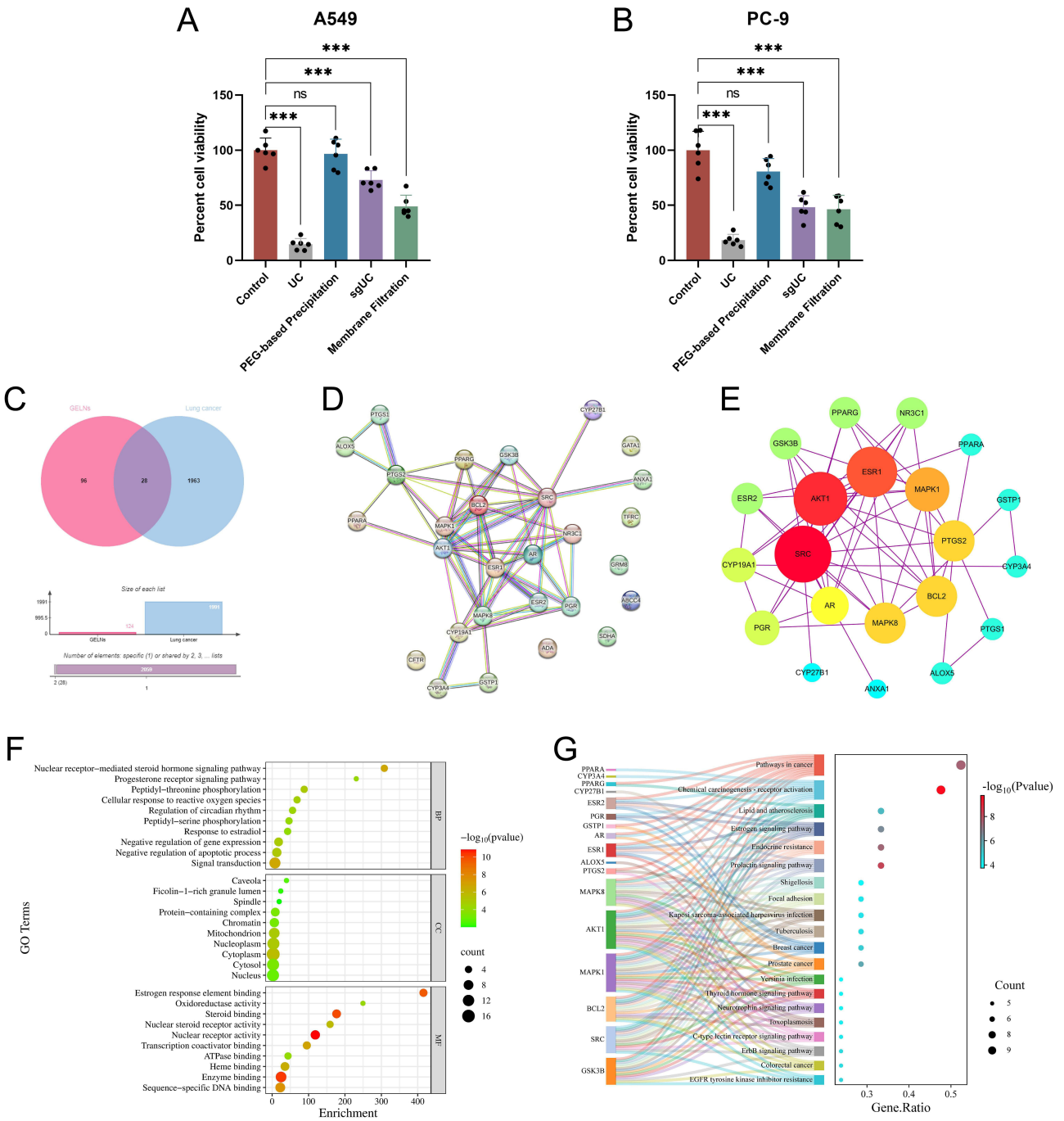

Figure 6 Network pharmacology analysis of GELNs in lung cancer. (**A** and **B**) Cell viability of A549 (**A**) and PC-9 (**B**) cells after 24 h treatment with GELNs isolated by four methods, as determined by the CCK-8 assay (n = 6, ns: non-significant, ***$p < 0.001$, compared with control). (**C**) The venn diagram illustrating the overlapping targets between GELNs and lung cancer. (**D**) The PPI network of the common targets. (**E**) The ranked PPI network after confidence-based screening, sorted by degree value. (**F**) GO enrichment analysis ($p < 0.05$). (**G**) KEGG enrichment analysis of the top 20 signaling pathways ($p < 0.05$).

degree values. Figure 6E presents the PPI network illustrating the interactions among these 21 key targets. KEGG pathway enrichment analysis and GO functional enrichment analysis were conducted on the 21 key targets using the DAVID database. Figure 6F displays the top 10 GO enrichment analysis bubble plots exhibiting the most significant differences, covering three categories: BP, CC, and MF. Figure 6G depicts the KEGG pathway enrichment analysis results for GELNs in lung cancer inhibition, which primarily involve the Estrogen signaling pathway and Prolactin signaling pathway.

Table 2 The Top 10 Main Active Metabolites in the GELNs

Number	Metabolite	Formula	Pubchem_ID	Number of Targets
1	Inositol	$C_6H_{12}O6$	892	19
2	L-Leucine	$C_6H_{13}NO_2$	6106	20
3	10-Gingerol	$C_{21}H_{34}O_4$	168115	15
4	[6]-Dehydrogingerdione	$C_{17}H_{22}O_4$	9796015	9
5	(2S)-2-hydroxybutanedioic acid	$C_4H_6O_5$	222656	20
6	Hexahydrocurcumin	$C_{21}H_{26}O_6$	5318039	23
7	Piperidine-2-Carboxylic Acid	$C_6H_{11}NO_2$	849	1
8	Adenosine	$C_{10}H_{13}N_5O_4$	60961	29
9	L-Valine	$C_5H_{11}NO_2$	6287	23
10	Maoyerabdosin	$C_{24}H_{36}O_9$	101920419	3

Results of Molecular Docking

The 21 core targets were plotted in the KM plotter database to generate survival curves for lung cancer patients. The results indicated that Estrogen Receptor 1(ESR1), Glycogen Synthase Kinase-3β (GSK3B), Glutathione S-transferase Pi 1 (GSTP1), Mitogen-Activated Protein Kinase 1 (MAPK1), Mitogen-Activated Protein Kinase 8 (MAPK8), Nuclear Receptor Subfamily 3 Group C Member 1 (NR3C1), Progesterone Receptor (PGR), and SRC Proto-Oncogene, Non-Receptor Tyrosine Kinase (SRC) genes were closely associated with the survival of lung cancer patients. As shown in Figure S4A–H, overall survival of lung cancer patients was positively correlated with expression of ESR1, NR3C1, and PGR, and negatively correlated with the other five genes. Based on these findings, these eight genes were selected for further in-depth research.

In this study, molecular docking was performed to assess the interactions between 10 major GELNs-derived metabolites and 8 key targets relevant to lung cancer. A binding affinity of less than −5 kcal/mol was considered indicative of favorable binding, while a value below −7 kcal/mol signified a highly stable interaction. As detailed in Figure 7A, Adenosine, 10-Gingerol, Hexahydrocurcumin, [6]-Dehydrogingerdione, and Maoyerabdosin exhibited stable binding with most of the proteins. Given that 10-Gingerol, Hexahydrocurcumin, and [6]-Dehydrogingerdione are primary pharmacological constituents of ginger, we selected them for further investigation. The proteins GSK3B, PGR, and SRC, which demonstrated stable binding with all three compounds, were subjected to binding mode visualization, the results of which are presented in Figure 7B–J.

Results of Molecular Dynamics Simulation

MD simulations were employed to validate the molecular docking results of 10-Gingerol, Hexahydrocurcumin, and [6]-Dehydrogingerdione with the proteins GSK3B, PGR, and SRC (Figures 8A–I and S4A–I). Comprehensive analyses of root-mean-square deviation (RMSD), radius of gyration (Rg), root-mean-square fluctuation (RMSF), binding distance, and buried solvent-accessible surface area (Buried SASA) revealed that the protein-small molecule ligand complexes overall exhibited favorable structural integrity and binding stability over the 100 ns MD simulation. Although complexes underwent conformational adjustments in the initial phase, they achieved stability in the later stage of the simulation. The global conformation of the protein-ligand complexes exhibited no significant deviation. Furthermore, the overall structure of the protein-ligand complexes remained compact, with no unfolding or loose conformations observed. The ligands were stably anchored in the protein binding pockets, with no significant displacement of the binding sites and stable binding modes. The binding interfaces between proteins and ligands maintained close contact, and non-covalent interactions (eg, hydrophobic interactions and hydrogen bonds) remained stable throughout the simulation, which provided crucial support for the stable binding of the complexes.

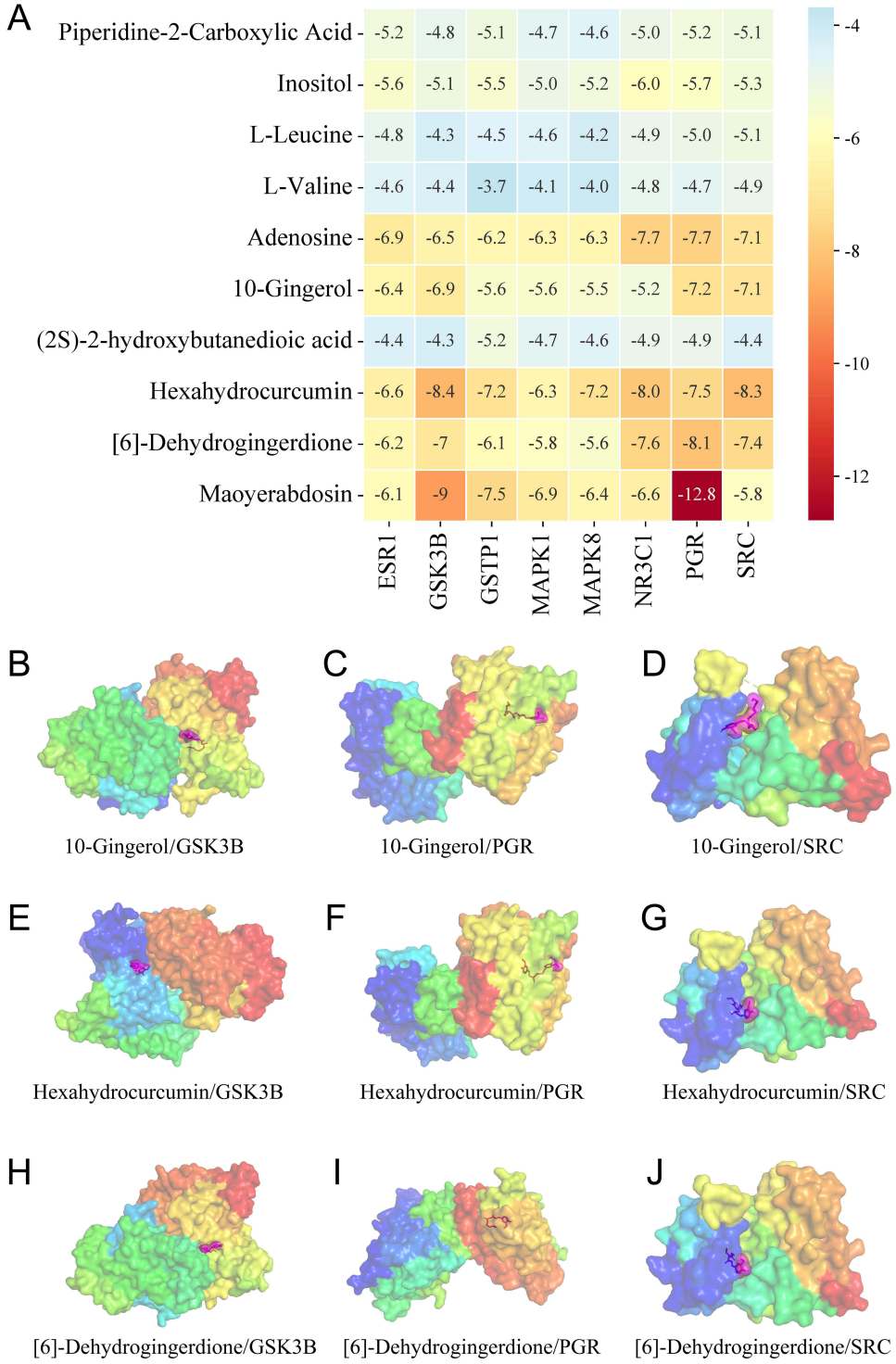

Figure 7 Docking results of major metabolites and the key targets. (**A**) Specific binding energy values. (**B, E** and **H**) Visualization of molecular docking of GSK3B protein with 10-gingerol, Hexahydrocurcumin, and [6]-Dehydrogingerdione, respectively. (**C, F** and **I**) Visualization of molecular docking of PGR protein with 10-gingerol, Hexahydrocurcumin, and [6]-Dehydrogingerdione, respectively. (**D, G** and **J**) Visualization of molecular docking of SRC protein with 10-gingerol, Hexahydrocurcumin, and [6]-Dehydrogingerdione, respectively.

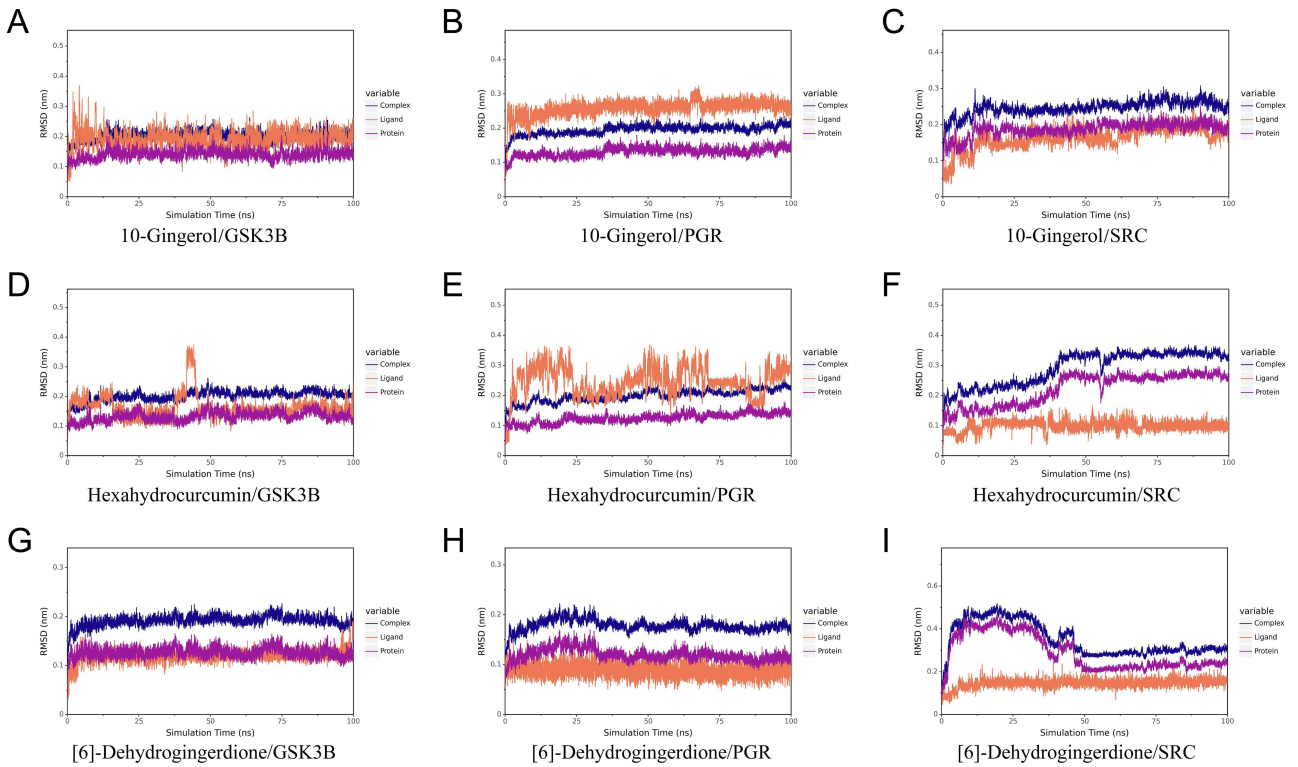

Figure 8 Visualization of RMSD results from molecular dynamics simulation. (**A**–**C**) RMSD results of 10-gingerol binding to GSK3B, PGR, and SRC, respectively. (**D**–**F**) RMSD results of Hexahydrocurcumin binding to GSK3B, PGR, and SRC, respectively. (**G**–**I**) RMSD results of [6]-Dehydrogingerdione binding to GSK3B, PGR, and SRC, respectively.

Discussion

Exosomes have gained significant attention as a key area of research, demonstrating considerable promise for both revealing pathophysiological mechanisms of diseases and developing novel nanomedicines.[37] Nevertheless, achieving high-purity isolation and precise purification of these nanoscale particles is a critical step enabling in-depth functional and application-oriented studies. Although several reports have indicated that isolation methods affect the efficiency, purity, and content of MEs, there is a notable scarcity of research regarding their effects on the extraction of PELNs.[38] In our study, all four methods successfully isolated GELNs. Under TEM, GELNs extracted by all four methods exhibited the characteristic exosome-like morphology. However, GELNs have their own characteristics in terms of yield, particle size distribution, and zeta potential.

UC proved to be the most effective method for obtaining a high mass yield of GELN protein. However, the NTA data indicate that this high-yield sample had a relatively broad size distribution, with the lowest percentage (64.36±0.99%) of particles within the typical 30–150 nm exosome range. Crucially, these particles exhibited the highest negative zeta potential (−26.37±1.22 mV), suggesting a superior colloidal stability due to strong electrostatic repulsion, which is often associated with a cleaner surface charge less shielded by co-precipitated contaminants. In stark contrast, the membrane filtration method yielded the lowest protein mass and a relatively low absolute value of zeta potential (−11.03±0.33 mV), yet paradoxically produced the highest particle concentration. This apparent discrepancy could be attributed to compromised vesicular integrity during filtration, potentially due to shear forces, leading to the generation of ruptured or "empty" vesicles. These vesicular would be counted by NTA but contain minimal protein, thereby explaining the low protein yield.[39] sgUC demonstrated an excellent balance in purifying GELNs. A significant majority (78.22±2.97%) of the isolated particles fell within the characteristic size range of 30–150 nm, representing a marked improvement in size homogeneity over the UC method. Critically, this enhancement in purity was achieved without a substantial sacrifice in yield. Furthermore, the zeta potential of −17.0±0.29 mV suggests that the sgUC protocol successfully removes a substantial portion of charged impurities. Collectively, these findings indicate that sgUC excels in delivering GELNs

https://doi.org/10.2147/IJN.S541948

with high purity. In contrast, the PEG-based precipitation method, while yielding a high quantity of proteins, generated particles with the least negative zeta potential (−9.3±0.67 mV). This strongly indicates the significant co-isolation of non-vesicular materials.

We further evaluated the stability of GELNs isolated by the four methods, beginning with an assessment of their stability in saline solutions. In 0.9% NaCl, GELNs extracted by UC and sgUC remained relatively stable in the short term. However, in 10% NaCl, the particle size of GELNs isolated by all four methods increased, with the membrane filtration method showing the most pronounced change. Exosomes possess a lipid bilayer membrane, which is a semipermeable structure. This membrane allows water molecules to pass through freely, while the passage of larger molecules or ions, such as salt ions, is considerably slower or entirely restricted.[40] Under the hypertonic conditions of 10% NaCl, the membranes of GELNs undergo shrinkage and deformation, leading to compromised integrity and altered surface properties.[41] The reduction in electrostatic repulsion allows van der Waals attractive forces to dominate when particles collide via Brownian motion, causing irreversible aggregation into large clusters.[42] This mechanism likely explains the observed increase in particle size of GELNs in 10% NaCl. Notably, GELNs isolated by membrane filtration, which may already be structurally compromised during extraction, exhibited the most significant size increase, possibly due to their heightened susceptibility to aggregation under osmotic stress.

In the study investigating the stability of GELNs isolated by four different methods in FBS, a particularly interesting observation was made. Upon initial introduction into FBS, the particle size of GELNs in all four groups decreased significantly compared to their size in other solvents, returning to the standard size range for exosomes. Over time, the particle size of GELNs isolated by UC and membrane filtration remained constant. In contrast, the particle size of GELNs obtained through sgUC and PEG-based precipitation continuously increased. During our stability assessment of GELNs, we employed DLS for particle size analysis. Since DLS measures the collective fluctuation of scattered light from the entire population, it is highly susceptible to the presence of large particles or aggregates.[43] Consequently, in our results, the particle size of GELNs detected by DLS may be overestimated due to the formation of aggregates within the system. FBS constitutes a complex protein system where serum proteins (such as albumin) can rapidly adsorb onto the surface of GELNs, forming a "protein corona".[44] This process shifts the stabilization mechanism of the system from "electrostatic stabilization" to "steric stabilization",[45] thereby preventing the aggregation of GELNs driven by van der Waals forces. As a result, the particle size detected by DLS more closely approximates their true dimensions. While the overly purified and potentially modified surface of sgUC-isolated GELNs leads to unstable protein corona interactions, the PEG-based method introduces numerous non-vesicular impurities that hinder the formation of a stable corona. This indicates that the UC and membrane filtration methods are more suitable for clinical research, as they can avoid adverse events such as vascular occlusion caused by particle aggregation or allergic reactions induced by PEG. This finding holds significant implications for the clinical investigation of GELNs and provides substantial reference value for the clinical development of other PELNs. When GELNs isolated by the four methods were stored at 25°C, 4°C, −20°C, and −80°C, a general increase in particle size was observed, likely due to particle aggregation. Notably, storage at −80°C resulted in minimal change in particle size, suggesting it as a potentially suitable storage temperature for preserving GELNs integrity.

Furthermore, we performed a comparative analysis of the composition of GELNs isolated by the four methods using non-targeted metabolomics. Non-targeted metabolomics identified a core metabolome of 649 components shared across GELNs extracted by the four distinct methods, representing their stable constitutive profile. However, quantitative differences were observed in the abundance of some shared components. Furthermore, each isolation method yielded GELNs containing unique metabolites not detected in the other method. Although GELNs extracted by all four methods were successfully internalized by lung cancer cells, their inhibitory effects on the cancer cells varied significantly. This functional variation is likely attributable to their distinct compositional profiles. For instance, UC-isolated GELNs, which exhibited the most potent anti-lung cancer activity, were found to be enriched with 10-Gingerol and 1-Dehydro-6-gingerdione among their top 10 most abundant constituents. Notably, 10-Gingerol affects multiple metastatic processes and induces apoptosis in MDAMB-231 breast cancer cells.[46] Similarly, 1-Dehydro-6- gingerdione has been shown to inhibit tumor growth by promoting the ferroptosis pathway in breast cancer.[47] The relatively low abundance of these active constituents in GELNs isolated by sgUC and membrane filtration may account for their diminished anti-

proliferative efficacy against lung cancer cells. However, GELNs isolated by PEG-based precipitation exhibited no anti-proliferative effect at the experimental concentrations. This insufficient efficacy is most likely attributed to the fact that this method will co-precipitate multiple impurities, such as free proteins, resulting in the formation of large polymer aggregates,[48] or the hydrophobic environment caused by PEG affects the physiological activity of GELNs. These aggregates dilute the effective dosage of the GELNs themselves and, in turn, interfere with their intended pharmacological activity.

Based on our previous findings, we employed network pharmacology to systematically investigate the potential mechanisms by which GELNs exert anti-lung cancer effects. Furthermore, molecular docking and MD simulations were utilized to analyze the specific binding interactions between the core metabolites and their key targets. Our results indicated that the anti-lung cancer activity of GELNs is closely associated with 3 bioactive components (10-Gingerol, Hexahydrocurcumin, and [6]-Dehydrogingerdione) and three key targets (GSK3B, PGR, and SRC). Existing studies have demonstrated that 10-Gingerol, Hexahydrocurcumin, and [6]-Dehydrogingerdione exhibit significant inhibitory effects on tumor cells. Specifically, Wang et al observed that Hexahydrocurcumin suppresses hepatocellular carcinoma progression by targeting the TRIM23/MBNL1 axis.[49] And Hsu et al revealed that [6]-Dehydrogingerdione induces cell cycle arrest and apoptosis in breast cancer cells via the reactive oxygen species (ROS)/c-Jun N-terminal kinase (JNK) pathway.[50] Notably, the targets GSK3B, PGR, and SRC are closely implicated in the occurrence and progression of lung cancer. Zheng et al reported that modulation of GSK3B can disrupt the progression of non-small cell lung cancer.[51] Zhao et al demonstrated that high expression of PGR exerts a potent preventive effect against lung cancer in both in vitro and in vivo models.[52] And Que et al indicated that SRC inhibitors represent promising therapeutic strategies for disrupting tumor clustering and improving clinical outcomes in patients with metastatic lung cancer.[53] Via molecular docking and MD simulations, we observed that 10-Gingerol, Hexahydrocurcumin, and [6]-Dehydrogingerdione can bind stably to GSK3B, PGR, and SRC. This finding suggests that these three bioactive components may inhibit lung cancer initiation by modulating the activity of GSK3B, PGR, and SRC.

Conclusion

In conclusion, this study establishes that while multiple methods can isolate GELNs, UC emerged as the optimal extraction method for GELNs in experimental research, yielding GELNs with high protein integrity, superior stability, and the most potent anti-lung cancer activity. This study reveals that the anti-proliferative activity of UC-isolated GELNs against lung cancer cells may be mediated through the regulation of GSK3B, PGR, and SRC by key bioactive components including 10-Gingerol, Hexahydrocurcumin, and [6]-Dehydrogingerdione. This study, however, has certain limitations. For instance, due to experimental constraints, DLS was employed instead of the more precise NTA for characterizing particle size during the stability assessment. Furthermore, the investigation into the anti-lung cancer mechanisms of GELNs remains incomplete, as it lacks validation through in vivo studies. Nevertheless, membrane filtration technology holds substantial promise for its commercial development, and the introduction of tangential flow filtration could be a viable strategy to mitigate structural damage during processing.

Ethics Statement

The ginger used in this study were authenticated as *Zingiber officinale* Roscoe by Prof. Hubiao Chen. A voucher specimen (Voucher number: HKBU-ZO-2024-003) has been deposited at the Dr. and Mrs. Hung Hin Shiu Museum of Chinese Medicine, Hong Kong Baptist University. This research strictly adheres to intemational and domestic ethical guidelines and legal regulations governing the use of human data. Since the study utilized publicly available data with patient informed consent already obtained by the database provider, it was deemed exempt from additional ethical approval under the Measures for Ethical Review of Life Science and Medical Research Involving Human Subjects (China, 2023, Article 32, ltems 1 and 2).

Acknowledgments

The authors would like to thank the Electron Microscopy Center, Biomedical Research Institute, Hubei University of Medicine for providing TEM services for the characterization of GELNs in this work. We also thank the staff of Honest Biotechnology Co., LTD. (Wuhan, China) for providing support for metabolomics experiments.

Author Contributions

All authors made a significant contribution to the work reported, whether that is in the conception, study design, execution, acquisition of data, analysis and interpretation, or in all these areas; took part in drafting, revising or critically reviewing the article; gave final approval of the version to be published; have agreed on the journal to which the article has been submitted; and agree to be accountable for all aspects of the work.

Funding

This research was funded by the Sanming Project of Medicine in Shenzhen (No. SZZYSM202106004), the National Natural Science Foundation of China (No. 82272960), the Basic Research Project of Baoan District Science and Technology Plan (No. 2023JD255), the Guangdong Provincial Administration of Traditional Chinese Medicine (No. 20252037), the Open Project of Hubei Key Laboratory of Wudang Local Chinese Medicine Research, Hubei University of Medicine (No. WDCM2024024, WDCM2024008), the Scientific and Technological Project of Shiyan City of Hubei Province (No. 24Y141), and Caojunling National Veteran Pharmaceutical Worker Inheritance Studio.

Disclosure

The authors declare no competing interests or conflicts of interest in this work.

References

1. Johnstone RM, Adam M, Hammond JR, et al. Vesicle formation during reticulocyte maturation. Association of plasma membrane activities with released vesicles (exosomes). *J Biol Chem*. 1987;262(19):9412–9420. doi:10.1016/S0021-9258(18)48095-7
2. Lai JJ, Chau ZL, Chen SY, et al. Exosome processing and characterization approaches for research and technology development. *Adv Sci*. 2022;9(15):e2103222. doi:10.1002/advs.202103222
3. Kimiz-Gebologlu I, Oncel SS. Exosomes: large-scale production, isolation, drug loading efficiency, and biodistribution and uptake. *J Control Release*. 2022;347:533–543. doi:10.1016/j.jconrel.2022.05.027
4. Kalluri R, LeBleu VS. The biology, function, and biomedical applications of exosomes. *Science*. 2020;367(6478):eaau6977. doi:10.1126/science.aau6977
5. Sadeghi S, Tehrani FR, Tahmasebi S, et al. Exosome engineering in cell therapy and drug delivery. *Inflammopharmacology*. 2023;31(1):145–169. doi:10.1007/s10787-022-01115-7
6. Zhang M, Hu S, Liu L, et al. Engineered exosomes from different sources for cancer-targeted therapy. *Signal Transduct Target Ther*. 2023;8(1):124. doi:10.1038/s41392-023-01382-y
7. Rehman FU, Liu Y, Zheng M, et al. Exosomes based strategies for brain drug delivery. *Biomaterials*. 2023;293:121949. doi:10.1016/j.biomaterials.2022.121949
8. Tenchov R, Sasso JM, Wang X, et al. xosomes─nature's lipid nanoparticles, a rising star in drug delivery and diagnostics. *ACS Nano*. 2022;16(11):17802–17846. doi:10.1021/acsnano.2c08774
9. Rezaie J, Feghhi M, Etemadi T. A review on exosomes application in clinical trials: perspective, questions, and challenges. *Cell Commun Signal*. 2022;20(1):145. doi:10.1186/s12964-022-00959-4
10. Mu N, Li J, Zeng L, et al. Plant-derived exosome-like nanovesicles: current progress and prospects. *Int J Nanomed*. 2023;18:4987–5009. doi:10.2147/IJN.S420748
11. Dad HA, Gu TW, Zhu AQ, et al. Plant exosome-like nanovesicles: emerging therapeutics and drug delivery nanoplatforms. *Mol Ther*. 2021;29(1):13–31. doi:10.1016/j.ymthe.2020.11.030
12. Hwang JH, Park YS, Kim HS, et al. Yam-derived exosome-like nanovesicles stimulate osteoblast formation and prevent osteoporosis in mice. *J Control Release*. 2023;355:184–198. doi:10.1016/j.jconrel.2023.01.071
13. Kilasoniya A, Garaeva L, Shtam T, et al. Potential of plant exosome vesicles from grapefruit (Citrus × paradisi) and tomato (Solanum lycopersicum) juices as functional ingredients and targeted drug delivery vehicles. *Antioxidants*. 2023;12(4):943. doi:10.3390/antiox12040943
14. Yin L, Yan L, Yu Q, et al. Characterization of the MicroRNA profile of ginger exosome-like nanoparticles and their anti-inflammatory effects in intestinal Caco-2 cells. *J Agric Food Chem*. 2022;70(15):4725–4734. doi:10.1021/acs.jafc.1c07306
15. Yan L, Cao Y, Hou L, et al. Ginger exosome-like nanoparticle-derived miRNA therapeutics: a strategic inhibitor of intestinal inflammation. *J Adv Res*. 2025;69:1–15. doi:10.1016/j.jare.2024.04.001
16. Kumar A, Sundaram K, Teng Y, et al. Ginger nanoparticles mediated induction of Foxa2 prevents high-fat diet-induced insulin resistance. *Theranostics*. 2022;12(3):1388–1403. doi:10.7150/thno.62514
17. Anusha R, Ashin M, Priya S. Ginger exosome-like nanoparticles (GELNs) induced apoptosis, cell cycle arrest, and anti-metastatic effects in triple-negative breast cancer MDA-MB-231 cells. *Food Chem Toxicol*. 2023;182:114102. doi:10.1016/j.fct.2023.114102

18. Sung H, Ferlay J, Siegel RL, et al. Global cancer statistics 2020: GLOBOCAN estimates of incidence and mortality worldwide for 36 cancers in 185 countries. *CA Cancer J Clin*. 2021;71(3):209–249. doi:10.3322/caac.21660
19. Raimondo S, Naselli F, Fontana S, et al. Citrus limon-derived nanovesicles inhibit cancer cell proliferation and suppress CML xenograft growth by inducing TRAIL-mediated cell death. *Oncotarget*. 2015;6(23):19514–19527. doi:10.18632/oncotarget.4004
20. Zhu LJ, Chen XQ, Lin QY, Feng JN, Yuan SF. Ginseng-derived exosomes attenuate immune evasion in NSCLC via PD-L1 modulation. *Cancer Manag Res*. 2025;17:1503–1512. doi:10.2147/CMAR.S540462
21. Zhu H, He W. Ginger: a representative material of herb-derived exosome-like nanoparticles. *Front Nutr*. 2023;10:1223349. doi:10.3389/fnut.2023.1223349
22. Man F, Meng C, Liu Y, et al. The study of ginger-derived extracellular vesicles as a natural nanoscale drug carrier and their intestinal absorption in rats. *AAPS Pharm Sci Tech*. 2021;22(6):206. doi:10.1208/s12249-021-02087-7
23. Zhang M, Viennois E, Prasad M, et al. Edible ginger-derived nanoparticles: a novel therapeutic approach for the prevention and treatment of inflammatory bowel disease and colitis-associated cancer. *Biomaterials*. 2016;101:321–340. doi:10.1016/j.biomaterials.2016.06.018
24. Zhao L, Zhang H, Li N, et al. Network pharmacology, a promising approach to reveal the pharmacology mechanism of Chinese medicine formula. *J Ethnopharmacol*. 2023;309:116306. doi:10.1016/j.jep.2023.116306
25. Bai G, Pan Y, Zhang Y, et al. Research advances of molecular docking and molecular dynamic simulation in recognizing interaction between muscle proteins and exogenous additives. *Food Chem*. 2023;429:136836. doi:10.1016/j.foodchem.2023.136836
26. Yan H, Li PH, Zhou GS, et al. Rapid and practical qualitative and quantitative evaluation of non-fumigated ginger and sulfur-fumigated ginger via Fourier-transform infrared spectroscopy and chemometric methods. *Food Chem*. 2021;341(Pt 1):128241. doi:10.1016/j.foodchem.2020.128241
27. Li P, Kaslan M, Lee SH, et al. Progress in exosome isolation techniques. *Theranostics*. 2017;7(3):789–804. doi:10.7150/thno.18133
28. Sung J, Yang C, Viennois E, et al. Isolation, purification, and characterization of Ginger-derived Nanoparticles (GDNPs) from ginger, rhizome of zingiber officinale. *Biol Protoc*. 2019;9(19):e3390. doi:10.21769/BioProtoc.3390
29. Suresh AP, Kalarikkal SP, Pullareddy B, Sundaram GM. Low pH-based method to increase the yield of plant-derived nanoparticles from fresh ginger rhizomes. *ACS Omega*. 2021;6(27):17635–17641. doi:10.1021/acsomega.1c02162
30. Ming T, Yang Y, Shang B, et al. Understanding mechanisms of Polygonatum sibiricum-derived exosome-like nanoparticles against breast cancer through an integrated metabolomics and network pharmacology analysis. *Front Chem*. 2025;13:1559758. doi:10.3389/fchem.2025.1559758
31. Iriawati I, Vitasasti S, Rahmadian FNA, Barlian A. Isolation and characterization of plant-derived exosome-like nanoparticles from Carica papaya L. fruit and their potential as anti-inflammatory agent. *PLoS One*. 2024;19(7):e0304335. doi:10.1371/journal.pone.0304335
32. Zu M, Xie D, Canup BSB, et al. 'Green' nanotherapeutics from tea leaves for orally targeted prevention and alleviation of colon diseases. *Biomaterials*. 2021;279:121178. doi:10.1016/j.biomaterials.2021.121178
33. Kong X, Liu C, Zhang Z, et al. BATMAN-TCM 2.0: an enhanced integrative database for known and predicted interactions between traditional Chinese medicine ingredients and target proteins. *Nucleic Acids Res*. 2024;52(D1):D1110–D1120. doi:10.1093/nar/gkad926
34. Győrffy B. Integrated analysis of public datasets for the discovery and validation of survival-associated genes in solid tumors. *Innovation*. 2024;5(3):100625. doi:10.1016/j.xinn.2024.100625
35. Liu Y, Yang X, Gan J, Chen S, Xiao ZX, Cao Y. CB-Dock2: improved protein-ligand blind docking by integrating cavity detection, docking and homologous template fitting. *Nucleic Acids Res*. 2022;50(W1):W159–W164. doi:10.1093/nar/gkac394
36. Li J, Zhang Y, Peng D, et al. Integrating UPLC-Q-TOF-MS, network pharmacology, molecular docking, and molecular dynamics simulation to reveal the material basis and mechanism of Xiangshao sanjie oral liquid in treating hyperplasia of mammary glands. *J Pharm Biomed Anal*. 2025;266:117074. doi:10.1016/j.jpba.2025.117074
37. Zhang Y, Bi J, Huang J, Tang Y, Du S, Li P. Exosome: a review of its classification, isolation techniques, storage, diagnostic and targeted therapy applications. *Int J Nanomed*. 2020;15:6917–6934. doi:10.2147/IJN.S264498
38. Tang YT, Huang YY, Zheng L, et al. Comparison of isolation methods of exosomes and exosomal RNA from cell culture medium and serum. *Int J Mol Med*. 2017;40(3):834–844. doi:10.3892/ijmm.2017.3080
39. Kim K, Park J, Jung JH, et al. Cyclic tangential flow filtration system for isolation of extracellular vesicles. *APL Bioeng*. 2021;5(1):016103. doi:10.1063/5.0037768
40. Frallicciardi J, Melcr J, Siginou P, Marrink SJ, Poolman B. Membrane thickness, lipid phase and sterol type are determining factors in the permeability of membranes to small solutes. *Nat Commun*. 2022;13(1):1605. doi:10.1038/s41467-022-29272-x
41. Zhang Y, Lin C. Lipid osmosis, membrane tension, and other mechanochemical driving forces of lipid flow. *Curr Opin Cell Biol*. 2024;88:102377. doi:10.1016/j.ceb.2024.102377
42. de Lange N, Leermakers FAM, Kleijn JM. Self-limiting aggregation of phospholipid vesicles. *Soft Matter*. 2020;16(9):2379–2389. doi:10.1039/C9SM01692A
43. Filipe V, Hawe A, Jiskoot W. Critical evaluation of Nanoparticle Tracking Analysis (NTA) by NanoSight for the measurement of nanoparticles and protein aggregates. *Pharm Res*. 2010;27(5):796–810. doi:10.1007/s11095-010-0073-2
44. Dridi N, Jin Z, Perng W, Mattoussi H. Probing protein corona formation around gold nanoparticles: effects of surface coating. *ACS Nano*. 2024;18(12):8649–8662. doi:10.1021/acsnano.3c08005
45. Bashiri G, Padilla MS, Swingle KL, Shepherd SJ, Mitchell MJ, Wang K. Nanoparticle protein Corona: from structure and function to therapeutic targeting. *Lab Chip*. 2023;23(6):1432–1466. doi:10.1039/D2LC00799A
46. Fuzer AM, Martin ACBM, Becceneri AB, da Silva JA, Vieira PC, Cominetti MR. [10]-gingerol affects multiple metastatic processes and induces apoptosis in MDAMB- 231 breast tumor cells. *Anticancer Agents Med Chem*. 2019;19(5):645–654. doi:10.2174/1871520618666181029125607
47. Tran THM, Dhandapani S, Abdus S, Kim YJ. 1-Dehydro-6-Gingerdione exerts anticancer effects on MDA-MB-231 cells and in the xenograft mouse model by promoting the ferroptosis pathway. *Phytother Res*. 2024;38(12):5901–5917. doi:10.1002/ptr.8331
48. Huang Q, Wang J, Ning H, Liu W, Han X. Exosome isolation based on polyethylene glycol (PEG): a review. *Mol Cell Biochem*. 2025;480(5):2847–2861. doi:10.1007/s11010-024-05191-x
49. Wang M, Weng C, Xu J, Xu K. Hexahydrocurcumin suppresses hepatocellular carcinoma by regulating TRIM23/MBNL1 pathway. *Sci Rep*. 2025;15(1):22541. doi:10.1038/s41598-024-82982-8

50. Hsu YL, Chen CY, Hou MF, et al. 6-Dehydrogingerdione, an active constituent of dietary ginger, induces cell cycle arrest and apoptosis through reactive oxygen species/c-Jun N-terminal kinase pathways in human breast cancer cells. *Mol Nutr Food Res*. 2010;54(9):1307–1317. doi:10.1002/mnfr.200900125
51. Zheng S, Xie Z, Zhou Z, et al. Intervening non-small-cell lung cancer progression by cell membrane coated platycodin D via regulating Hsa-miR-1246/FUT9/GSK3β pathway. *Int J Nanomed*. 2025;20:1661–1678. doi:10.2147/IJN.S479675
52. Zhao Y, Weng CC, Tong M, Wei J, Tai HH. Restoration of leukotriene B(4)-12- hydroxydehydrogenase/15-oxo-prostaglandin 13-reductase (LTBDH/PGR) expression inhibits lung cancer growth in vitro and in vivo. *Lung Cancer*. 2010;68(2):161–169. doi:10.1016/j.lungcan.2009.06.011
53. Que ZJ, Yang Y, Liu HT, et al. Jinfukang regulates integrin/Src pathway and anoikis mediating circulating lung cancer cells migration. *J Ethnopharmacol*. 2021;267:113473.